Electronic Letters on Computer Vision and Image Analysis 13(3):63-80; 2014

Blind Restoration of Motion Blurred Barcode Images using Ridgelet Transform and Radial Basis Function Neural Network

Shamik Tiwari*, Vidhya Prasad Shukla*, S. R. Biradar+, Ajay Kr. Singh *

** Faculty of Engineering & Technology, Mody University of Science & Technology, India*

+ SDM College of Engineering, Hubli-Dharwad, India

Received 22th Dec 2013; accepted 15th Oct 2014

Abstract

The aim of any image restoration techniques is to recover the original image from the degraded observation. One of the most common degradation phenomena in images is motion blur. In case of blind image restoration accurate estimation of motion blur parameters is required for deblurring of such images. This paper proposed a novel technique for estimating the parameters of uniform motion blur using ridgelet transform. Initially, the energy of ridgelet coefficients is used to estimate the blur angle and then blur length is estimated using a radial basis function neural network. This work is tested on different barcode images with varying parameters of blur. The simulation results show that the proposed method improves the restoration performance.

Key Words: Image Restoration, Motion Blur, Ridgelet Transform, Radial Basis Function Neural Network, Barcode Images.

1 Introduction

The barcode is one of the automatic identification technologies applied successfully in the world. Almost every consumer product has a unique one dimensional (1-D) or two dimensional (2-D) barcode for identification. Barcodes encode a series of characters or symbols to hold explicit information and a database key. With the use of a barcode laser scanner, product information such as manufacturing details and price can be easily accessed. Consumer can obtain information about a product at home or in a supermarket, with a scanning device that can decode the barcode, and a communication device that retrieves the information from a consumer product server. The ease of use of mobile phones with camera facility gives a portable platform for decoding barcode rather than the use of the traditional laser scanner which has lack of portability [1, 2]. Camera phones can take an image of the barcode and after that it can communicate to a consumer product server to access information related with the product. However, using a camera phone in such applications is challenging due to factors such as geometric distortion, noise, and blurring. Image blurring is frequently an issue that affects the performance of a barcode identification system.

Correspondence to: <shamiktiwari@hotmail.com>
http://dx.doi.org/10.5565/rev/elcvia.577
Recommended for acceptance by <Xavier Otazu>
ELCVIA ISSN: 1577-5097
Published by Computer Vision Center / Universitat Autonoma de Barcelona, Barcelona, Spain

Two main causes of blurring are motion and defocus blur [3, 4]. Motion blur appears due to the relative motion between the camera and object while the defocus blur appears due to the inaccurate focal length adjustment at the time of image capturing. Blurring induces the degradation of image quality, specifically for barcode images where the encoded information is easily lost due to blur. An image deconvolution technique refers as non-blind deconvolution, if blur kernel information is available. In case of blind deconvolution [5], blur kernel is not known. Blind image deconvolution problem has been categorized into two groups. In the first group, we can put those methods, in which the point spread function (PSF) of blur is estimated in first step and then degraded image is restored using any of the classical restoration methods such as Wiener filtering in subsequent step. In the methods of second group, PSF estimation and image restoration are achieved simultaneously. The work presented in this paper falls in the former category, where PSF parameters are estimated before image restoration.

Cannon [6] proposed a technique to identify the blur parameters using power spectrum of many sub images by dividing blurred image into different blocks. Fabian et al. [7] proposed a method based on Cannon's method. Initially, they applied spectral subtraction method to reduce high level noise then transformed improved spectral magnitude function to cepastral domain for identification of blur parameters. Chang et al. [8] proposed a method using the bispectrum of blurred image. In this method blur parameters are obtained using the central slice of the bispectrum. Rekleitis [9] suggested a method to estimate the optical flow map of a blurred image using information from the motion blur. He applied steerable filters to estimate motion blur angle and 1-D cepstrum to find blur length. Yitzhaky et al. [10] used autocorrelation function of derivative image based on the examination that image characteristics along the direction of motion blur remain dissimilar from the characteristic in other directions. Lokhande et al. [11] estimated parameters of motion blur by using periodic patterns in Frequency domain. They proposed blur direction identification using Hough transform and blur length estimation by collapsing the 2-D spectrum into 1-D spectrum. Aizenberg et al. [12] presented a work that identifies blur type, estimates blur parameters and perform image restoration using neural network. Ratnakar et al. [13] offered an approach to estimate the motion blur parameters using Gabor filter for blur direction and Radial Basis Function Neural Network (RBFNN) for blur length with sum of Fourier coefficients as features. Dobes et al. [14] presented a fast method of finding motion blur length and direction. This method computes the power spectrum of the image gradient in the frequency spectrum. The orientation of blur is found using Radon transform and the distance between the neighbouring stripes in power spectrum is used to estimate the blur length. Finally, the image is deblurred using estimated parameters and Lucy-Richardson algorithm. Fang et al. [15] proposed another method consisting of Hann windowing and histogram equalization as pre-processing steps. Jian-Feng et al. [16] developed an approach based on Framelet for blind deblurring of motion blurred image. Wang et al. [17] presented the concept of quasi-cepstrum. They estimated uniform linear motion blur kernel parameters using amplitude spectrum and quasi-cepstrum. Ratnakar et al. [18] modeled the blur length detection problem as a multiclass classification problem and used support vector machine. Shamik et al. [19] compared the performance of various parameter estimation techniques and showed that performance of the existing algorithms deteriorate in noisy conditions.

Though there are large amount of work reported, no method is completely accurate. Researchers are still active in this field, in order to improve the restoration performance by searching for robust method of blur parameters estimation. In this paper, we introduce a new multi-resolution feature extraction technique based on the discrete ridgelet transform. The theory of ridgelets revealed that it is very good at representing edges in comparison to wavelets which is an efficient transform for detecting point discontinuities but not efficient for the geometric properties of structures and regularity of edges. The ridgelet transform overcomes has been successfully used in object classification, seismic imaging, and image de-noising. However, we have not found any application of ridgelets for blur identification.

The rest of the paper is structured as follows. Section 2 describes the image degradation model. Section 3 and 4 briefly discuss ridgelet transform and radial basis function neural network. In section 5, the overall methodology is discussed. Section 6 presents the simulation results of parameter estimation. Section 7 discusses use deblurring algorithm. Finally in section 8, conclusions and future work are discussed.

2 Image Degradation Model

The image degradation process is modeled by the following convolution process [3, 4]

$$g(x,y) = f(x,y) * h(x,y) + \eta(x,y) \tag{1}$$

where $g(x,y)$ is the degraded image, $f(x,y)$ is the uncorrupted original image, $h(x,y)$ is the point spread function (PSF) that caused the degradation and $\eta(x,y)$ is the additive noise in spatial domain. Since, convolution in spatial domain is equal to the multiplication in frequency domain, equation (1) can be written as

$$G(u,v) = F(u,v)H(u,v) + N(u,v) \tag{2}$$

where $G(u,v)$is the degraded image, $F(u,v)$ is the uncorrupted original image, $H(u,v)$ is the optical transfer function that caused the degradation and $N(u,v)$ is the additive noise in frequency domain. In order to develop reliable blur detection, it is necessary to understand process of the image degradation. Degradation function may be due to improper opening and closing of shutter, atmospheric turbulence, out of focus of lens or due to motion blur. The noise and degradation functions have contradicting effects on the image spectrum. The degradation function produces averaging effect on the image data and act as low pass filters, whereas noise often introduces additive broad band signals in the image data.

When an object or the camera is moved during light exposure, a motion blurred image is produced. The motion blur can be in the form of translation, rotation, and sudden change of the scale or some combinations of these forms. When the scene to be recorded translates relative to the camera at a constant velocity ($v_{relative}$) under an angle of θ radians with the horizontal axis during the exposure interval [0, $t_{exposure}$], the distortion is one dimensional. Defining the length of motion as $L = v_{relative} \times t_{exposure}$, the PSF for uniform motion blur in spatial domain can be described as

$$h(x,y) = \begin{cases} \frac{1}{L} \; if \; \sqrt{x^2+y^2} \leq \frac{L}{2} \; and \; \frac{x}{y} = -\tan\theta \\ 0 \qquad\qquad \text{otherwise} \end{cases} \tag{3}$$

The frequency response of *h,* is a SINC function given by

$$H(u,v) = sinc\big(\pi L(u\cos\theta + v\sin\theta)\big) \tag{4}$$

The PSF estimation techniques are applied to estimate two parameters length (L) and angle (θ). In this work we have considered the uniform motion blur and ignore the additive noise in image restoration model.

3 Ridgelet Transform

Images are generally described via orthogonal, non-redundant transforms like wavelet or discrete cosine transform. Wavelets provide a strong method to identify point singularities but these are not able to represent singularities along lines efficiently. Radon transform is the dominant method to detect lines. Ridgelet can be viewed as a wavelet analysis in Radon domain so the ridgelet transform achieves very robust representation of linear singularities of images [20]. Hence, ridgelet transform in image analysis is attractive since singularities are often joined together along edges or contours in images. Therefore, they can offer an important contribution in order to detect and represent lines, which are fundamental structures in spectrum of motion blurred images. Arivazhagan et al. [21] used features derived from sub-bands of the ridgelet decomposition for classification of texture images. Huang et al. [22] proposed a rotation invariant feature based on the combination of ridgelet, a directional non-separable wavelet transform, and Fourier transforms for texture classification. Suoping et al. [23] proposed a method which extracts wave direction from sea surface images based on ridgelet transform. Zhang et al. [24] presented a method which calculates approximately swash velocity from near shore video images. In this work a computational algorithm based on ridgelet transform is proposed. Energy of ridgelet coefficients is calculated using variance statistics and a peak angle is extracted as the direction of the linear feature of wave swash fronts. Given an integrable bivariate function $f(x,y)$, its continuous ridgelet transform (CRT) in $\mathbf{R}^2$ is defined by [25]

$$CRT_f(s,l,\theta) = \int_{-\infty}^{\infty}\int_{-\infty}^{\infty} \varphi_{s,l,\theta}(x,y) f(x,y) dx\, dy \tag{5}$$

For each $s > 0$, each $l \in \boldsymbol{R}$ and each $\theta \in [0, 2\pi)$. This function is constant along lines $x\cos\theta + y\sin\theta = const$. Where the ridgelet basis function $\varphi_{s,l,\theta}(x,y)$ in 2-D is defined from a wavelet-type 1-D function $\varphi(x)$ as

$$\varphi_{s,l,\theta}(x,y) = \frac{1}{\sqrt{s}}\varphi\left(\frac{x\cos\theta + y\sin\theta - l}{s}\right) \tag{6}$$

The CRT appears same as 2-D continuous wavelet transform (CWT) except that the point parameters of wavelet i.e. (x,y) are replaced by line parameters i.e. (ρ,θ). In other words, the basis function of multiscale wavelet and ridgelet transform are related as

Wavelet: $\varphi_{scale,\ point-position}$, Ridgelet: $\varphi_{scale,\ line-position}$

As a consequence, wavelets are very efficient to represent isolated point singularities, whereas ridgelets are very efficient to signify singularities along lines. In fact, one can observe ridgelets as an approach of concatenating 1-D wavelets along lines. In 2-D, points and lines are linked via the Radon transform, consequently the wavelet and ridgelet transforms are linked via the Radon transform in ridgelet transform. The Radon transform for an image $f(x,y)$ is the collection of line integrals indexed by $(l,\theta) \in \boldsymbol{R} \times [0, 2\pi)$ and is given as

$$R_f(\rho,\theta) = \int_{-\infty}^{\infty}\int_{-\infty}^{\infty} f(x,y)\delta(x\cos\theta + y\sin\theta - \rho)dx\, dy \tag{7}$$

where δ is the dirac distribution. Thus, the ridgelet transform can be represented in terms of the Radon transform as

$$CRT_f(s,l,\theta) = \int_{-\infty}^{\infty} \varphi_{s,l}(\rho) R_f(\rho,\theta) d\rho \tag{8}$$

where θ stands for the orientation of Radon transform and ρ is a variable parameter measures perpendicular distance of a line from origin. Therefore, the basic approach for calculating the ridgelet transform is to take a 1-D wavelet transform along the slices (projections) in Radon space. According to projection-slice theorem Radon transform can be achieved by applying 1-D inverse Fourier transform to the 2-D Fourier transform restricted to radials lines passing through origin. A schematic diagram of the radon transform and ridgelet transform with relationship with various transforms is shown in Figures 1 and 2.

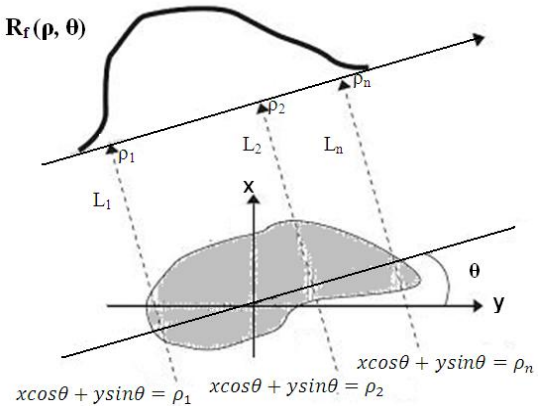

Figure 1: Radon Transform

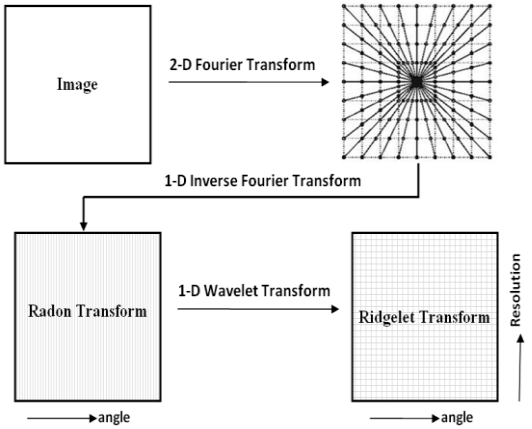

Figure 2: Ridgelet Transform

A sym4 wavelet with 4 level decomposition is used in this work. 'sym4' is used throughout the work because it gives the highest energy difference between sharp image and its blurred version in comparison to other wavelet filters like haar, db1, db2, sym2, coif1, coif2 and meyer with least number of coefficients. Symlets are also known as least asymmetrical (LA) wavelets because they are nearly but not exactly symmetrical. These are compactly supported wavelets with the highest number of vanishing moments for a given support width. In the standard notation symN, N is the order. The main property of this filter family is

the near-linear phase of its filters, when considered in terms of the frequency response. The phase function of the least asymmetric filters generated by the symlets have the smallest maximum deviation in frequency from the best fitting linear phase function. This is an excellent feature if we are concerned in an accurate localization of some incident like local phase coherence disrupt by blur.

4 Radial Basis Function Neural Network

Function approximation is a widely acceptable uses of artificial neural networks. Generally, in approximation problem deals with establishing a relation between one or more input variables and single output variable. Radial Basis Functions are initially used in the field of approximation theory for multivariable interpolation problems. Broomhead et al. [26] and Moody et al. [27] were the first to make use of the radial basis functions in the implementation of neural networks. Afterwards, RBFNN has wide range of applications, such as pattern classification [28], fault detection [29, 30], system identification [31], nonlinear function approximation [32], image restoration [33-35], speech recognition [36], and time-series prediction [37]. Basically these networks are feed-forward networks which use a supervised learning algorithm. It consists of a single hidden layer of one or multiple units whose activation function is Gaussian or some other basis kernel function. Regardless of similarity to back propagation in many respects, radial basis function networks have a number of advantages. The significant features of RBF neural networks are as follows.

i. Contain more compact topology [38].
ii. Universal predictors [39].
iii. Having best approximation property [40].
iv. Fast learning speed due to locally tuned neurons [27].

In general, a RBF neural net consists of three layers; where the first layer accepts input vectors, second layer consists of the radial basis functions as hidden layer and last layer gives output. The inputs of hidden layer are the linear combinations of scalar weights and the input vector $\boldsymbol{U} = [u_1, u_2, u_3, \ldots., u_n]^T$, where the scalar weights are usually assigned unity values. Thus, the whole input vector appears to each neuron in the hidden layer. The incoming vectors are mapping by the radial basis functions in each hidden node. The output layer yields a vector $\boldsymbol{V} = [v_1, v_2, v_3, \ldots \ldots v_m]^T$, for m outputs by linear combination of the outputs of the hidden nodes to produce the final output. The network output is obtained by

$$\boldsymbol{V} = f(\boldsymbol{U}) = \sum_{i=1}^{k} w_i \varphi_i(\boldsymbol{U}) \tag{9}$$

where $f(\boldsymbol{U})$ is the final output, $\varphi_i(\boldsymbol{U})$denotes the radial basis function of the *i*-th hidden node, w_i denotes the hidden-to-output weight corresponding to the *i*-th hidden node, and k is the total number of hidden nodes. A radial basis function is a multidimensional function that describes the distance between a given input vector and a pre-defined centre vector. There are different types of radial basis function. In this work, the standard Gaussian nonlinear basis function is used, which is defined as

$$\varphi_i(\boldsymbol{U}) = e^{-(\frac{\|x-\mu_i\|^2}{2\sigma_i^2})} \tag{10}$$

where μ_i and σ_i denote the center (mean) and spread width (standard deviation) of the *i*-th node, respectively.

5 Image Deblurring Algorithm

In the approach presented in this paper, a given blurred barcode image is analyzed to find out the angle and length of the motion blur. The blur is modeled with the help of these two motion blur parameters [41]. The blurring process can be viewed as a linear convolution of the original image with that blur kernel; and it can be removed by reversing this operation. First of all in a preprocessing step, a blurred image is resized to

256 × 256 to reduce the computation cost, and then a RGB image to the grayscale conversion is performed. As explained, in section 5.1 the blur direction is determined by performing a Ridgelet transform on the logarithmic power spectrum of the Hann windowed barcode image. Next, in section 5.2 the blur length is estimated using RBFNN as regression tool with energy of ridgelet coefficients as features. In the last step as explained in section 7, the PSF is calculated and Lucy-Richardson algorithm is applied to deconvolute the image. Figure 3 shows an overview of the motion deblurring algorithm.

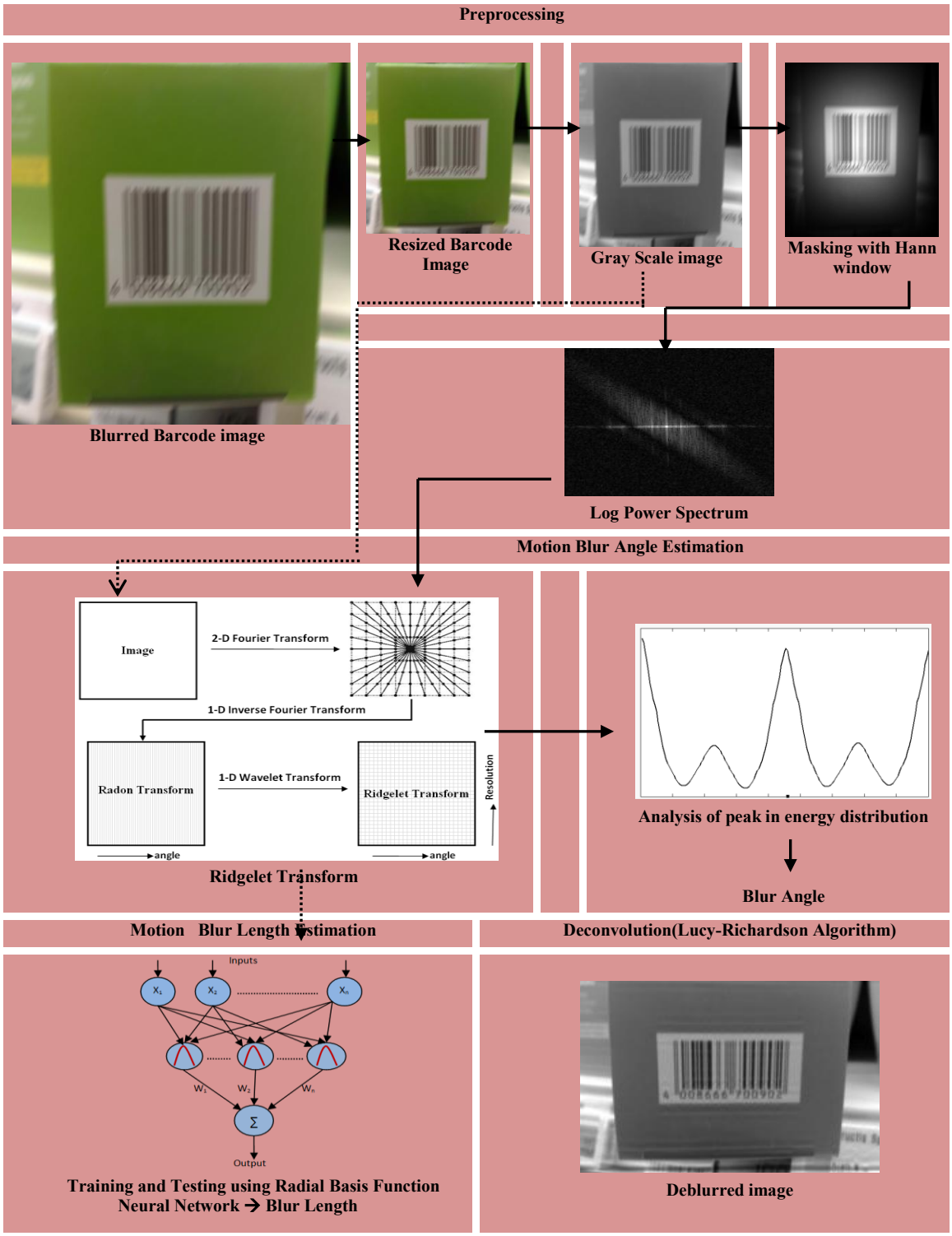

Figure 3: Overview of the image deblurring algorithm

5.1 Estimation of Motion Blur Angle

If we convert the blurred image in frequency domain, we can extract the motion blur parameters from Fourier spectrum. Figure 4 shows the effect of motion blur on the Fourier spectrum of original image. Frequency response of motion blurred image shows the dominant parallel lines orthogonal to the motion orientation with very low values [12, 13 and 14]. So, the task of estimating the motion orientation is analogous to the task of calculating orientation of these parallel lines. To find the line direction, we can apply Ridgelet transform.

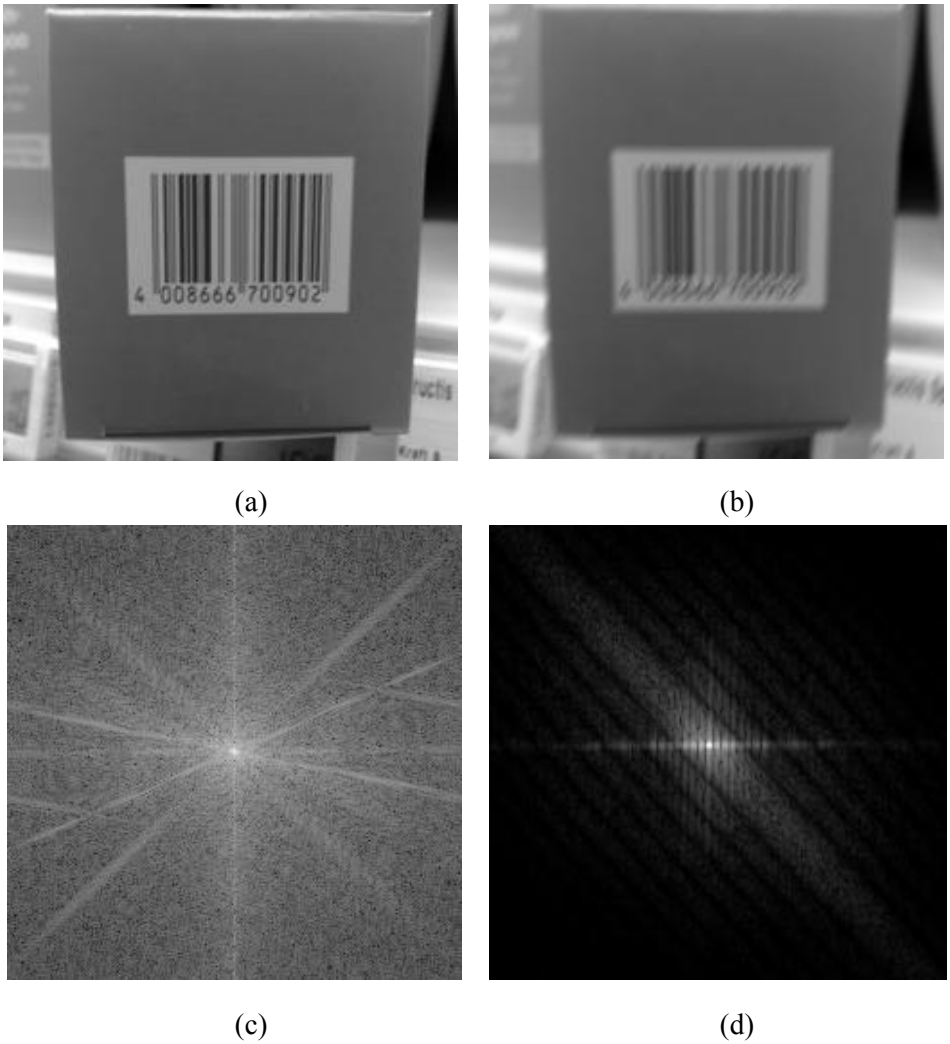

Figure 4: (a) Original image (b) Blurred image with motion length 10 pixels and motion orientation 45^0 (c) Fourier spectrum of original image (d) Fourier spectrum of blurred image

Radon transform of a function is bound to coincide with the direction of linear singularity. When image $f(x, y)$ is integrated along θ, linear singularities changed into point singularities. A 1-D wavelet is fully competent in detection of point singularities. In the same manner, ridgelet is able to detect singularities along lines. Ridgelet transform can efficiently detect the line feature. Applying the ridgelet transform to the image with linear features, when the direction of the straight line coincides with a certain ridgelet direction, the ridgelet energy along this direction has highest energy. Therefore, the energy of the projection at this direction is maximum. This technique can be used to determine line orientation in an image. To estimate the motion blur angle first find the logarithmic power spectrum of Hann windowed image. After that, the ridgelet transform in interval $[0, \pi)$ with 1° increments is computed to take a 1-D wavelet transform along

the slices in Radon domain of Fourier image. The energy (i.e., sum of coefficients) of the projection is calculated at all directions for the motion blurred barcode image with angle 45^0 and length 10. 4-level wavelet decomposition gives one approximation (ca4) and four detail coefficients (cd4, cd3, cd2 and cd1). Figures 5(a) to 5(e) demonstrate the energies for ca4, cd4, cd3, cd2 and cd1 components, respectively. The two components cd2 and cd1 with minimum energy caused mainly by image noises are discarded while sum of energies with ca4, cd4 and cd3 components is calculated. After above calculation, the peak of ridgelet coefficient energy is corresponding to motion blur angle. Figure 5 shows the energy of ridgelet coefficients at each angle for power spectrum of blurred image as given in Figure 4 (d). It is evident that peak of energies is at angle 45^0, which is the motion blur angle.

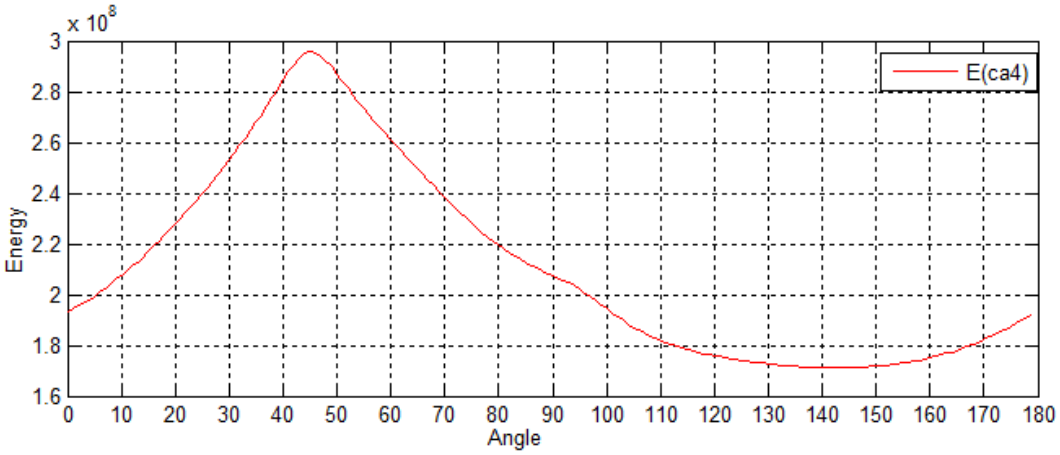

(a)

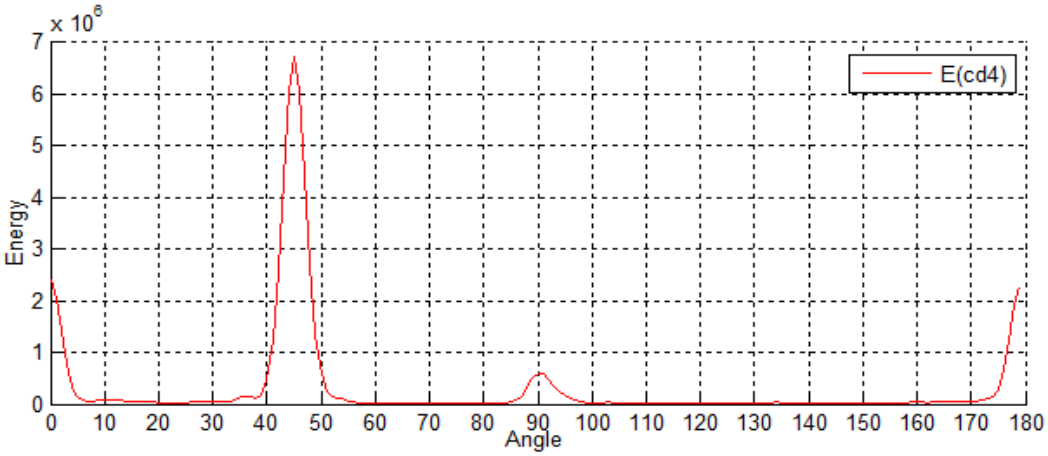

(b)

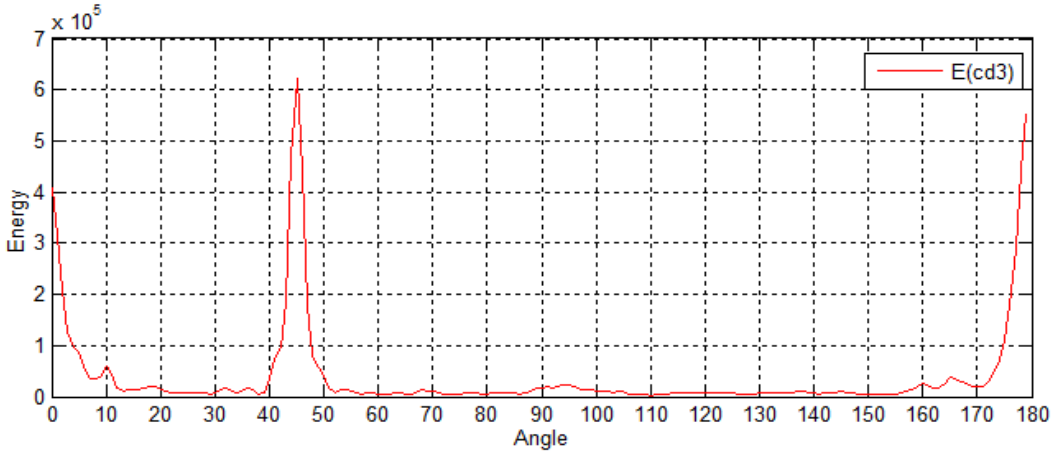

(c)

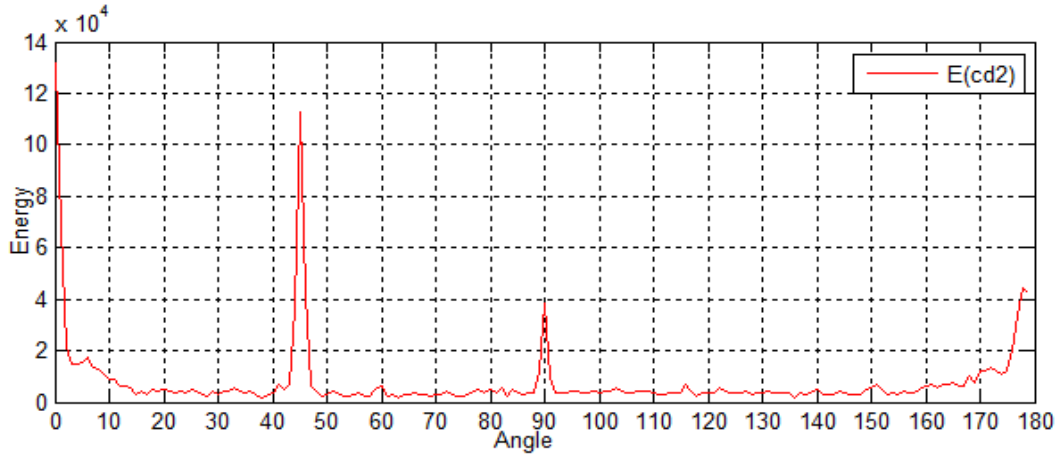

(d)

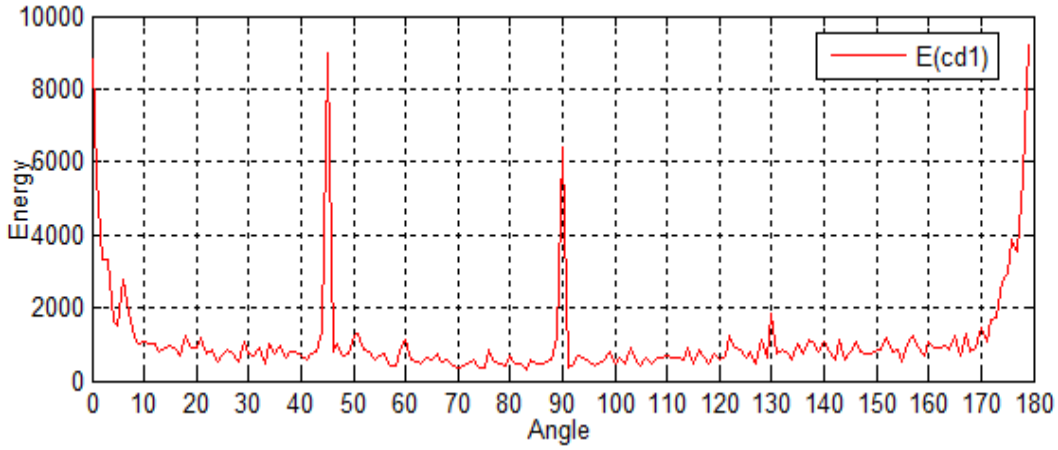

(e)

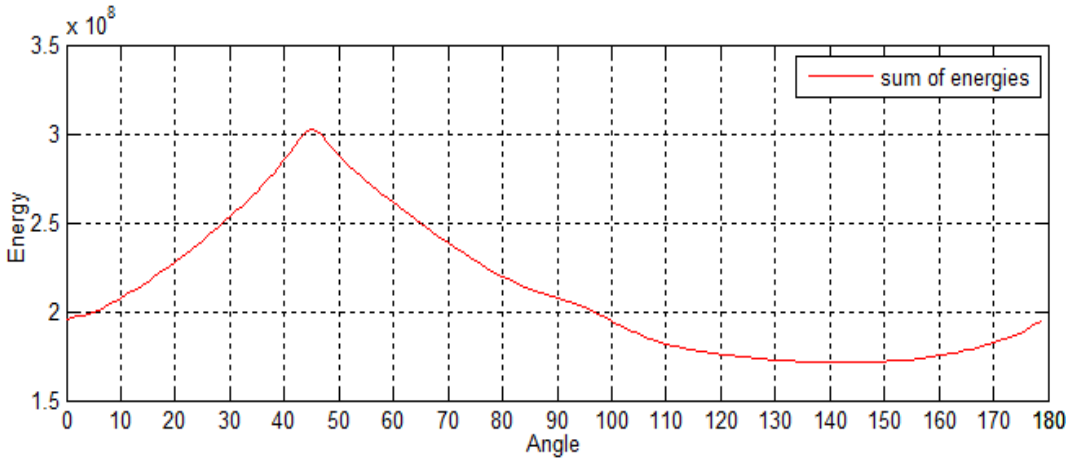

(f)

Figure 5: (a)-(e) Energy distribution of Ridgelet coefficients for ca4, cd4, cd3, cd2, and cd1 respectively. (f) sum of energies for ca4, cd4 and cd3

The motion blur angle detection algorithm can be summarized as follows

i. Preprocess the input blurred barcode image.
ii. Perform Hann Windowing over $f(x, y)$ to remove boundary artifacts.
iii. Compute the Fourier transform $F(u, v)$ of step2 image.

iv. Compute the log power spectrum of $F(u, v)$.
v. For a set of angles $\theta = \{\theta_1, \theta_2, \ldots\ldots\ldots\ldots\ldots, \theta_n\}$, where $\theta_i \in [0, \pi)$, with 1 degree spaced intervals, compute the normalized Radon vectors at these angles.
vi. Apply a 4-level 1-D DWT on the Radon vectors to obtain the ridgelet coefficients.
vii. Find the sum of energies of ridgelet coefficient for vectors of each orientation.
viii. Find the maximum energy which is corresponding to motion blur angle.

5.2 Estimation of Motion Blur Length

The steps of the algorithm for motion blur length identification are detailed in Figure 6. These are six major steps: image acquisition, preprocessing, ridgelet transform, calculation of mean energy, designing of RBFNN system and result analysis.

In the initial step, we have applied fast discrete ridgelet transform as explained in section three to pre-processed motion blurred barcode images. Once these transformed images acquired, the method demands the extraction of features. Therefore, the mean of energy for each decomposition (i.e. ca4, cd4, cd3, cd2, and cd1) have been calculated in the next step to prepare the training and testing database. Finally with this feature database training and testing performed using RBFNN. Ridgelet transform using 'sym4' wavelet filter of level 4 is applied to a barcode image to obtain its coefficients. These coefficients are then used to form the features of that image. After achieving the ridgelet coefficients the energy related with each scale independently. The energy of a scale is calculated by the sum of absolute values of ridgelet coefficients. So, we obtain a feature vector $\boldsymbol{E} = (E_1, E_2 \ldots\ldots\ldots, E_5)^T$ for each of the barcode image. We propose the use of feature vector E in order to establish the relationship between energy of ridgelet transform coefficients and motion blur length L.

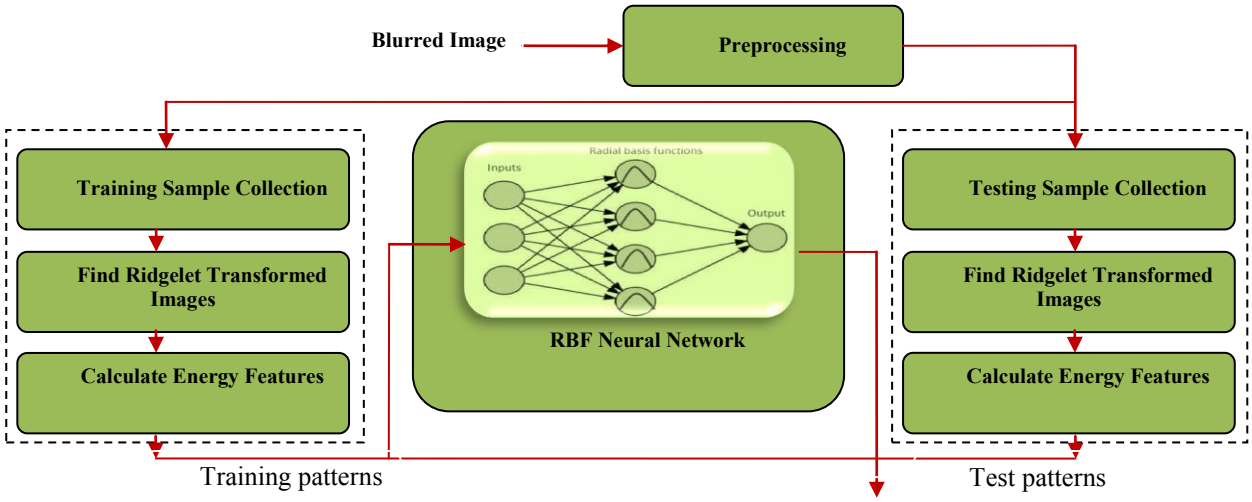

Figure 6: Motion blur length identification frame–work

An original barcode image as in Figure 4 (a) is blurred artificially by a uniform motion blur with parameter L whose value ranging from 1 to 20 and fixed angle of 0 degree. It is found that as the L increases, values of features in vector $\boldsymbol{E}$ decreases. The relationship between normalized features E_i and L are shown in Figure 7. It shows that when L increases these features decrease monotonously. So, we can estimate motion blur length from extracted energy features of the blurred image after establishing the relationship between $\boldsymbol{E}$ and L. Figures 8 and 9 show the plots using energy features E_1 and E_2 for three different images. Though, every image has the monotonous curve between E_i and L, but they are not superposed as shown in these figures. Therefore, for an unknown blurred image the value of L can not be estimated accurately because the curve of the given image is unknown.

It is evident from Figures 8 and 9 that incorrect results would be obtained, if any energy feature E_i of one image is used to estimate L according curve of another image. So that establishing the simple relationship between $\boldsymbol{E}$ and L is not sufficient to estimate motion parameter L of unknown image. It requires a complex

mapping between features and motion blur length with generalization ability. Neural networks can be used to resolve these issues. One of the significant features of neural nets is their ability to generalize. This reveals that a successfully trained neural network can classify data from the same class as the learning data that it has never seen before.

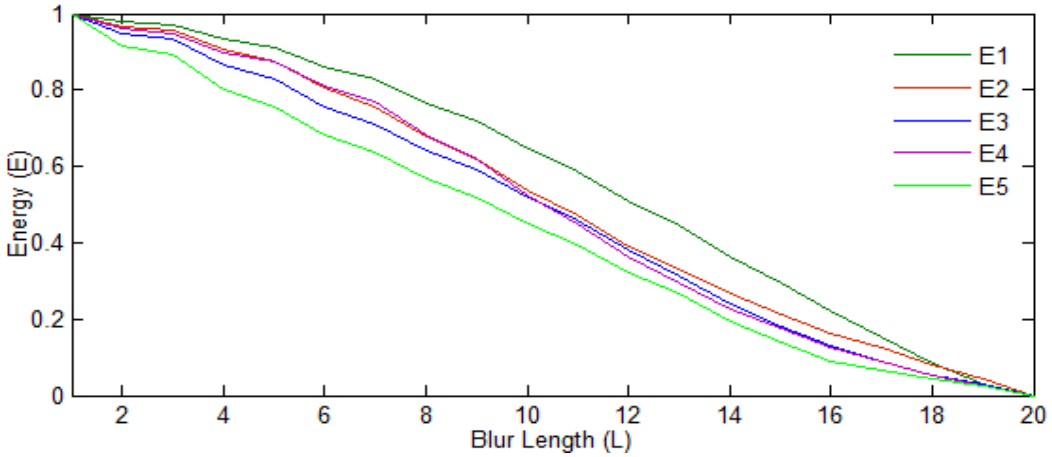

Figure 7: The relationship between $E_{1\text{-}5}$ and L

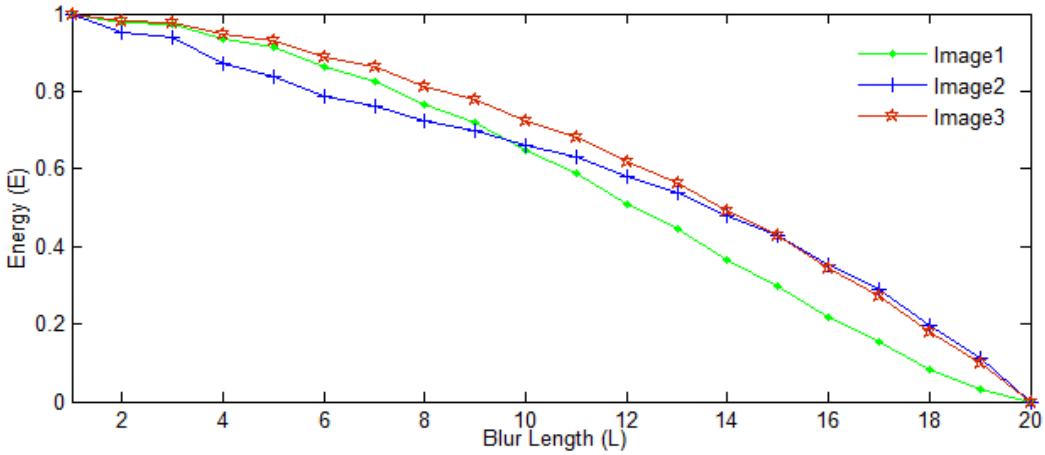

Figure 8: The relationship between energy feature E_1 and L for three different images.

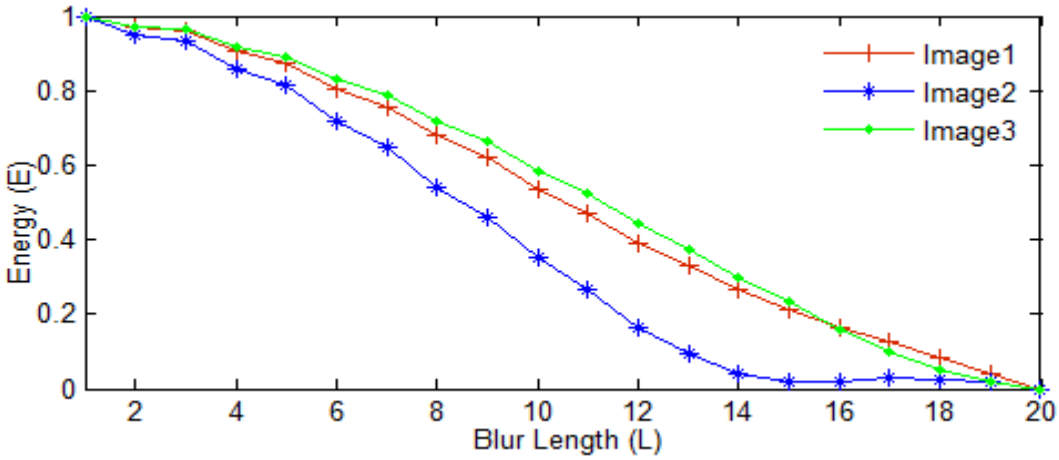

Figure 9: The relationship between energy feature E_2 and L for three different images.

6 Simulation Results

The performance of the proposed technique has been evaluated using many camera based 1-D barcode images. The WWU Muenster Barcode Database [44] of barcode images has been used in this work, which consist of numerous 1-D barcode images captured by camera. To carry out the experimental work, uniform motion blur is introduced synthetically in the barcode images. To test the proposed algorithm for angle estimation an example of barcode image shown in Figure10 was blurred from angle in the range [0, 180) with step size of 10^0. The estimated angles were recorded for image with motion lengths 10 and 20 pixels as in Figures 11(a) and 11(b). The results show accuracy over the methods proposed in [9], [11] and [13]. The tests are run on the same image for motion length estimation with varying length from 1 to 20 pixels with blur angle 0 and 90 degrees. We have used *newrbe* function available in Matlab neural network toolbox, which designs a radial basis network with zero error in the design vectors. The inputs to the RBF network neurons are the sum of energies features and output value is the blur length (L). *Newrbe* creates a precise model of neural networks, which can automatically decide the number of hidden layer, making predictions more accurate. The radius value (known as spread) of the function is varied for best performance of the RBF network. Principally, the larger spread is, the smoother the function approximation. Too large a spread means a lot of neurons are required to fit a fast-changing function. Too small a spread means many neurons are required to fit a smooth function, and the network might not generalize well. In this work, we have set the goal mse to 0.01 and tested the model for varying spread values in range .1 to 2. The spread value with best performance is found 1.2. The results shown in Figures 12(a) and 12(b) demonstrate robustness of proposed method in comparison to methods in [9] and [13].

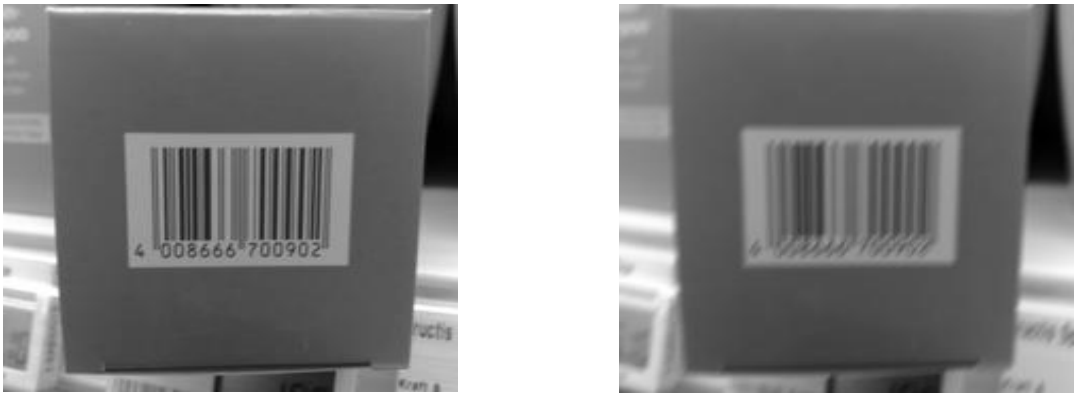

(a) (b)

Figure 10: The original barcode image (a) and an example of a blurred image (b) with the length of the motion blur is 20 pixels and $\theta = 30$ degree.

To carry out extensive experiment for motion blur angle estimation, we have selected first 15 barcode images from database. Then, all the images were artificially blurred with angle in the range [0, 180) with step of 10^0 and motion blur length 10 and 20 pixels. So, total 270 blurred images are formed synthetically. The estimated angles were recorded for all the images with motion lengths 10 and 20 pixels separately using the proposed method. Table 1 presents the summary of results. To carry out extensive experiment for motion blur length estimation, we have applied the proposed method on 50 1-D barcode images that were artificially degraded by lengths of motion blur in the range $1 \leq L \leq 20$ pixels with angle 0^0 and 90^0 separately. So, 1000 degraded images are obtained for each blur angle. Out of 1000 blurred images 500 images are used for training and all the images are utilized for testing. Table 2 presents the summary of results for length estimation. In these tables, the columns named "angle tolerance" and "length tolerance" illustrate the absolute value of errors (i.e. difference between the real values and the estimated values of the angle and length), respectively. The low values of the mean absolute error and standard deviation of errors show the high accuracy of our method in comparison to methods in [9] and [13].

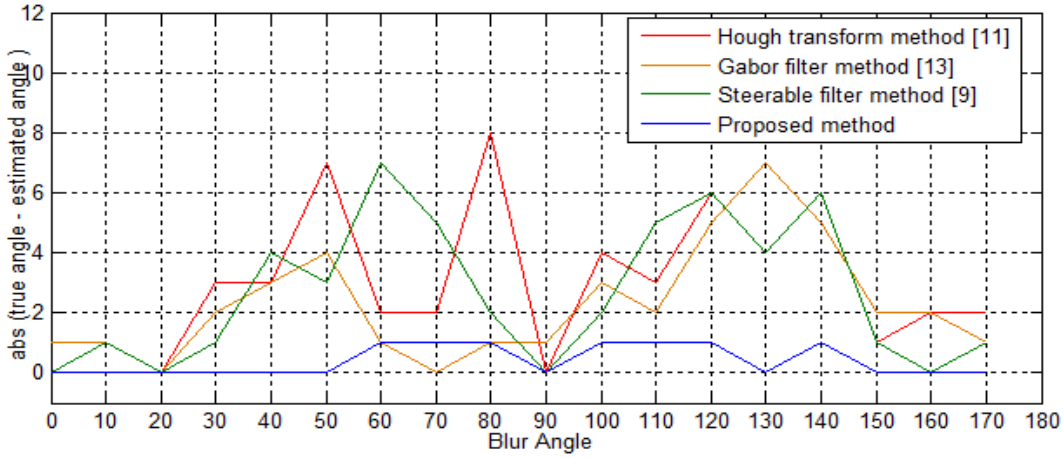

(a)

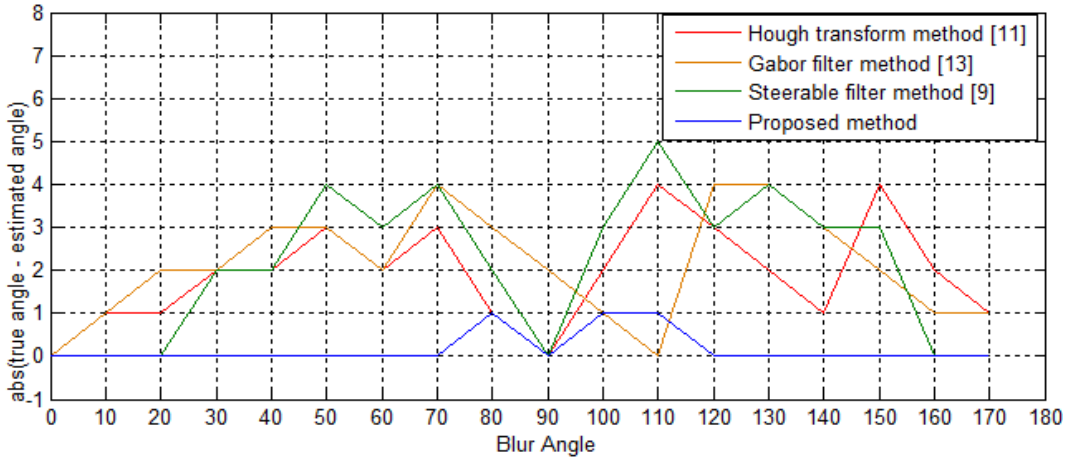

(b)

Figure 11: The average error in angle estimation for the Ridgelet transform and other methods. In (a) the motion blur length is10 pixels and in (b) the motion blur length is 20 pixels.

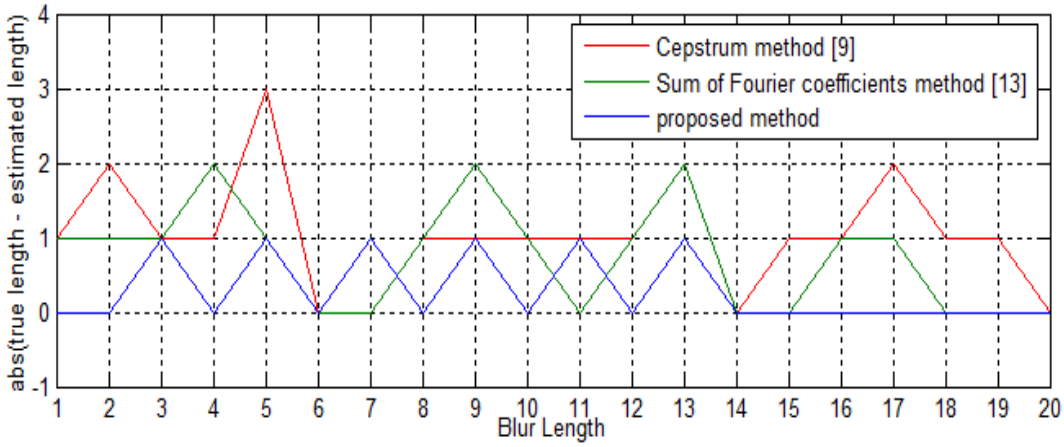

(a)

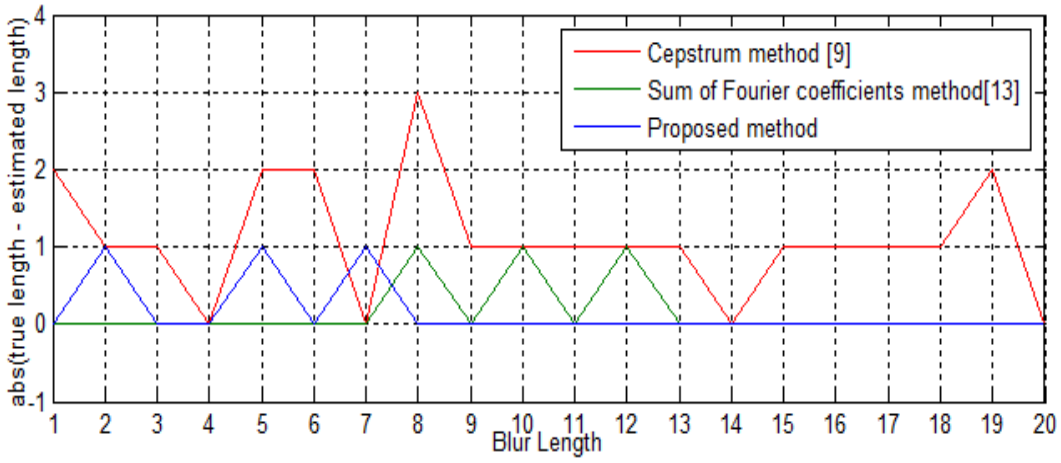

(b)

Figure12: The average error in length estimation for the Ridgelet transform and other methods. In (a) the motion blur angle is 0 degree and in (b) the motion blur angle is 90 degree.

Table 1: Simulation results of our and other algorithms on 270 degraded barcode images (256 × 256) for angle estimation with blur lengths 10 and 20 pixels

Cases	**Angle tolerance(in degree)**							
	Blur Length L=10				Blur Length L=20			
	Steerable filter method[9]	Hough transform method [11]	Gabor filter method [13]	Proposed method	Steerable filter method[9]	Hough transform method [11]	Gabor filter method [13]	Proposed method
Best estimate	0	0	0	0	0	0	0	0
Worst estimate	14	10	10	7	12	4	4	6
Average estimate	4.61	2.21	1.62	0.86	3.83	1.78	1.23	0.64
Standard deviation	3.13	1.81	0.92	1.31	2.65	1.34	.78	1.36

Table 2: Simulation results of proposed and other algorithms on 1000 degraded barcode images (256 × 256) with blur angles 0 and 90 degrees

Cases	**Length tolerance(in pixels)**					
	Blur angle θ=0 degree			Blur angle θ=90 degree		
	Sum of Fourier coefficients method[13]	Cepstrum method [9]	Proposed method	Sum of Fourier coefficients method[13]	Cepstrum method [9]	Proposed method
Best estimate	0	0	0	0	0	0
Worst estimate	3	3	1	2	3	1
Average estimate	0.40	0.56	0.01	0.33	0.54	0.03
Standard deviation	0.57	0.78	0.08	0.49	0.82	0.16

7 Image Deblurring

In the last step, we have applied the deblurring algorithm using the estimated parameters to remove the blur artefact. A significant application of blur parameters identification is image restoration. Estimated blur PSF can be used to deblur a blurred image. We use Lucy-Richardson (L-R) algorithm for deblurring. This algorithm is developed independently by [42] and [43] and it is a nonlinear and non-blind method.

The L-R has been derived from Bayesian probability hypothesis where image information is measured to be random quantities that are assumed to have a certain possibility of being formed from a family of other possible random quantities. The equation of the L-R algorithm is

$$f(x,y)^{n+1} = f(x,y)^n H^* \left(\frac{g(x,y)}{Hf(x,y)^n} \right) \tag{11}$$

where $f(x,y)^{n+1}$ is the new estimate from the previous one $f(x,y)^n$, $g(x,y)$ is the blurred image, n is the number of the step in the iteration, H is the blur filter (PSF) and H^* is the adjoint of H. In order to reduce noise amplification, which is a general problem of maximum likelihood methods, it is common practice to introduce a dampening threshold below which further iterations are (locally) suppressed. Otherwise high iteration numbers introduce artifacts to originally smooth image regions.

Figures 13(a-c) and 14(a-c) shows the restoration result of images using L-R method with estimated blur parameters after 10 and 15 iterations respectively. The images in Figures 13 and 14 clearly demonstrate that the reconstruction is able to produce good results. Text that could not even be identified as such becomes readable again, and individual elements of the barcodes become clearly distinguishable. Peak signal-to-noise ratio (PSNR in dB) is used as the quantitative parameter to evaluate the proposed scheme. The blurred image shown in Figure 13(b) has PSNR 15.32 dB, whereas after restoration as shown in Figure 13(c) has improved to 26.34 dB. The blurred image shown in Figure 14(b) has PSNR 17.84 dB, while after restoration as shown in Figure 14(c) has improved to 24.12 dB PSNR.

8 Conclusion

In this paper, we have proposed a proficient method for uniform motion blur parameter estimation for blind restoration of motion blurred barcode images. By considering the fact that barcode images have high linear singularities, ridgelet transform has been utilized in this method. The simulation results show the improved performance over other parameter estimating method. The main advantage of the suggested method is that it is more robust because ridgelet transform has an excellent high directional sensitivity and anisotropy for linear singularities in comparison to other direction filters. In future this work can be extended by considering the presence of noise in blurred images and real blurred images.

ACKNOWLEDGMENT

We highly appreciate Faculty of Engineering and Technology, Mody University of Science & Technology, Laxmangarh for providing facility to carry out this research work.

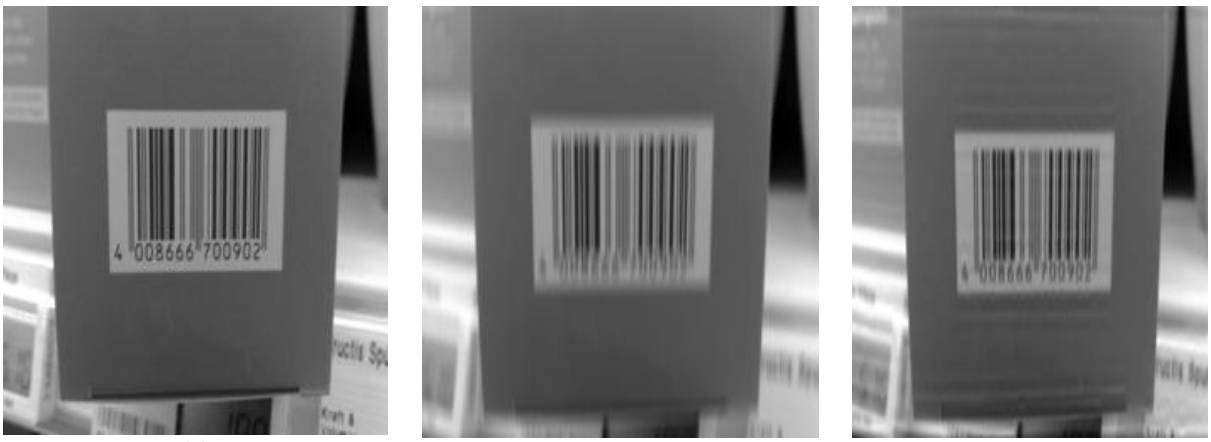

(a) (b) (c)

Figure13: (a) original barcode image, (b) an example of a blurred barcode image with the length of the blur as 10 pixels and θ = 90 degree (PSNR = 15.32 dB) and (c) restored barcode image using Lucy-Richardson algorithm after 10 iterations with estimated parameters length as 10 and θ = 91 degree (PSNR = 26.34 dB).

(a) (b) (c)

Figure14: (a) original barcode image, (b) an example of a blurred barcode image with the blur length as 15 pixels and θ = 30 degree (PSNR = 17.84 dB) and (c) restored barcode image using Lucy-Richardson algorithm after 15 iterations with estimated parameters length as 15 and θ = 25 degree (PSNR = 24.12 dB).

References

[1] K. Q. Wang, "Barcode character segmentation for mobile cameras", *Technical report of NOKIA*, 2003.

[2] J. Vartiainen, T. Kallonen, J. Ikonen, "barcodes and mobile phones as part of logistic chain in construction industry," *The 16th International Conference on Software, Telecommunication, and Computer Networks*, pp. 305-308, 2008. <http://dx.doi.org/10.1109/softcom.2008.4669500>

[3] A. K. Jain, *Fundamentals of Digital Image Processing*, Prentice Hall International, 1989.

[4] R. C. Gonzalez, R. E.Woods, *Digital Image Processing*, Prentice Hall, 2007.

[5] D. Kundur, D. Hatzinakos, "Blind image deconvolution", *IEEE Signal Processing Magazine*, vol. 13(3) pp. 43–64,1996. <http://dx.doi.org/10.1007/978-3-319-10485-0>

[6] M. Cannon, "Blind deconvolution of spatially invariance image blurs with phase," *IEEE Trans. Acoust. Speech Signal Proces*sing, vol. 24, 1976. <http://dx.doi.org/10.1109/tassp.1976.1162770>

[7] R. Fabian, D. Malah, "Robust identification of motion and out-of-focus blur parameters from blurred and noisy images", *CVGIP: Graphical Models and Image Processing*, vol. 53(5), pp. 403-412, 1991. <http://dx.doi.org/10.1016/1049-9652(91)90025-f>

[8] M. Chang, A. M. Tekalp, and T. A. Erdem. "Blur identification using the bispectrum," *IEEE Transactions on Signal Processing*, vol. 39(10), pp. 2323-2325, 1991. <http://dx.doi.org/10.1109/78.91207>

[9] I. M. Rekleitis, *Visual motion estimation based on motion blur interpretation*, MSc Thesis, School of Computer Science, McGill University, Montreal, Quebec, Canada, 1995.

[10] Y. Yitzhaky, N. S. Kopeika, "Identification of blur parameters from motion blurred images", *CVGIP: Graph Models and Image Processing*, vol. 59, pp. 310-320, 1997. <http://dx.doi.org/10.1006/gmip.1997.0435>

[11] R. Lokhande, K. V. Arya, P. Gupta, "Identification of blur parameters and restoration of motion blurred images", *ACM symposium on applied computing*, pp. 301-305, 2006. <http://dx.doi.org/10.1145/1141277.1141347>

[12] I. Aizenberg, D. V. Paliy, J. M. Zurada, J. T. Astola, "Blur identification by multilayer neural network based on multivalued neurons", *IEEE Transactions on Neural Networks*, vol. 19(5), pp. 883-898, 1998. <http://dx.doi.org/10.1109/tnn.2007.914158>

[13] Ratnakar Dash, Pankaj Kumar Sa, Banshidhar Majhi, "RBFN based motion blur parameter estimation", *IEEE International Conference on Advanced Computer Control*, pages 327-331, 2009. <http://dx.doi.org/10.1109/icacc.2009.98>

[14] Michal Dobeš, Libor Machala, Tomáš Fürst, "Blurred image restoration: A fast method of finding the motion length and angle", *Digital Signal Processing*, vol. 20(6), pp. 1677-1686, 2010. <http://dx.doi.org/10.1016/j.dsp.2010.03.012>

[15] Xianyong Fang, Hao Wu, Zhongbiao Wu, Bin Luo, "An improved method for robust blur estimation", *Information Technology Journal*, vol. 10, pp. 1709-1716, 2011. <http://dx.doi.org/10.3923/itj.2011.1709.1716>

[16] Jian-Feng Cai, Hui Ji, Chaoqiang Liu, Zuowei Shen, "Framelet-based blind motion deblurring from a single image", *IEEE Transactions on Image Processing*, vol. 21(2), pp. 562-572, 2012. <http://dx.doi.org/10.1109/tip.2011.2164413>

[17] L. Wang, H. Y. Zhang, S. L. Peng, "New explorations on cannon's contributions and generalized solutions for uniform linear motion blur identification", *Journal Of Computer Science And Technology,* vol. 27(1), pp. 174-186, 2012. <http://dx.doi.org/10.1007/s11390-012-1215-2>

[18] Ratnakar Dash, Pankaj Kumar Sa, Banshidhar Majhi, "Blur parameter identification using support vector machine", *ACEEE Int. J. on Control System and Instrumentation*, Vol. 03(2), 2012.

[19] Shamik Tiwari, Ajay Kr. Singh, V. P. Shukla, "Certain investigations on motion blur detection and estimation", *International Conference on Signal, Image and Video Processing, IIT Patna*, pp. 108-114, 2012.

[20] E. J. Candes and D. L. Donoho, "Ridgelets – a surprisingly effective non adaptive representation for objects with edges," *Curves and Surfaces, L. L. S al., ed., Nashville, TN, (Vanderbilt University Press)*, 1999.

[21] S. Arivazhagan, L. Ganesan, T. G. Subash Kumar, "Texture classification using ridgelet transform", *Sixth International Conference on Computational Intelligence and Multimedia Applications*, pp.321-326, 2005. <http://dx.doi.org/10.1109/iccima.2005.55>

[22] K. Huang, S. Aviyente, "Rotation invariant texture classification with ridgelet transform and fourier transform", *IEEE International Conference on Image Processing*, pp.2141-2144, 2006. <http://dx.doi.org/10.1109/icip.2006.312867>

[23] Suoping Zhang, Chuntian Zhang, "Application of ridgelet transform to wave direction estimation", *Congress on Image and Signal Processing*, vol.2, pp.690,693, 2008. <http://dx.doi.org/10.1109/cisp.2008.494>

[24] Suoping Zhang, Chuntian Zhang, Zhanhui Qi, "Wave swash velocity estimation using ridgelet transform", *9th International Conference on Electronic Measurement & Instruments*, pp.4-1078,4-1081, 2009. <http://dx.doi.org/10.1109/icemi.2009.5274124>

[25] E. J. Candes, L. Demanet, D. L. Donoho, L. Ying, "Fast discrete ridgelet transform", Technical Report, *CalTech*, 2005.

[26] D. S. Broomhead and David Lowe, "Multivariable functional interpolation and adaptive networks", *Complex Systems*, vol.2, pp.321-355, 1988.

[27] J. Moody, C. J. Darken, "Fast learning in networks of locally- tuned processing units", *Neural Computation*, vol. 1(2), pp. 281-294, 1989. <http://dx.doi.org/10.1162/neco.1989.1.2.281>

[28] J. Daugman, "Face and gesture recognition: overview", *IEEE Trans. on Pattern Analysis and machine Intelligence*, Vol. 19(7), pp. 675-676, 1997. <http://dx.doi.org/10.1109/34.598225>

[29] Y. J. Zhai and D. L. Yu, "Radial basis function based feedback control for air fuel ratio of spark ignition", *Proc. Instn Mech. Engrs, Part D: J. Automobile Engineering*, Vol. 222, pp. 415-428, 2007. <http://dx.doi.org/10.1243/09544070jauto614>

[30] Adnan Hamad, Dingli Yu, J. B. Gomm, Mahavir S. Sangha, "Radial basis function neural network in fault detection of automotive engines", *International Journal of Engineering, Science and Technology*,Vol. 2(10), pp. 1-8, 2010. <http://dx.doi.org/10.4314/ijest.v2i10.64007>

[31] G. P. Liu, V. Kadir kamanathan, S. A. Billings, "Stable sequential identification of continuous nonlinear dynamical systems by growing RBF networks", *Int. J. Contr.*, vol. 65, no. 1, pp. 53–69, 1996. <http://dx.doi.org/10.1080/00207179608921686>

[32] M. Powell, "Radial basis functions for multivariable interpolation: A review", *J.C. Mason and M.G. Cox, eds, Algorithms for Approximation*, pp.143-167, 1987.

[33] I. Cha, S. A. Kassam, "RBFN restoration of nonlinearly degraded images", *IEEE Trans. on Image Processing*, vol. 5(6), pp. 964-975, 1996. <http://dx.doi.org/10.1109/83.503912>

[34] Yugang Jiang, "Motioned image restoration using rbf network and kalman filter", *IEEE International Conference on Systems, Man and Cybernetics*, 2005.

[35] Su Li-yun, "Motioned image restoration using rbf network and iterative wiener filter in wavelet domain", *CISP'08 Congress on Image and Signal Processing*, 2008.

[36] M. Niranjan, F. Fallside, "Neural networks and radial basis functions in classifying static speech patterns", *Computer Speech and Language*, vol. 4, pp. 275-289, 1990. <http://dx.doi.org/10.1016/0885-2308(90)90009-u>

[37] M. Casdagli, "Nonlinear prediction of chaotic time series", *Physica D*, vol. 35, pp. 335-356, 1989. <http://dx.doi.org/10.1016/0167-2789(89)90074-2>

[38] S. Lee and R. M. Kil, "A Gaussian potential function network with hierarchically self-organizing learning", *Neural Networks*, vol. 4, pp. 207–224, 1991. <http://dx.doi.org/10.1016/0893-6080(91)90005-p>

[39] J. Park and J. Wsandberg, "Universal approximation using radial basis functions network", *Neural Comput.*, vol. 3, pp. 246–257, 1991. <http://dx.doi.org/10.1162/neco.1991.3.2.246>

[40] F. Girosi and T. Poggio, "Networks and the best approximation property", *Biol. Cybern.*, vol. 63, pp. 169–176, 1990. <http://dx.doi.org/10.1007/bf00195855>

[41] Shamik Tiwari, V P Shukla, S R Biradar, Ajay Kumar Singh, "Texture features based blur classification in barcode images", *I.J. Information Engineering and Electronic Business, MECS Publisher*, vol. 5, pp. 34-41**,** 2013. <http://dx.doi.org/10.5815/ijieeb.2013.05.05>

[42] W. H. Richardson, "Bayesian-based iterative method of image restoration", *J. Opt. Soc. Am.* 62 (1), pp. 55-60, 1972. <http://dx.doi.org/10.1364/josa.62.000055>

[43] L. Lucy, "An iterative technique for the rectification of observed distributions", *Astron. J.* 79, pp. 745, 1974. <http://dx.doi.org/10.1086/111605>

[44] S. Wachenfeld, S. Terlunen, X. Jiang. http://cvpr.uni-muenster.de/research/barcode.